Glutathione-Assisted Synthesis of Hierarchical PbS Via Hydrothermal Degradation and Its Application in the Pesticidal Biosensing

Xiaofang Shen, Zhaoxia Li, Yan Cui, Yuehong Pang[*]

State Key Laboratory of Food Science and Technology, School of Food Science and Technology, Jiangnan University, Wuxi, 214122, Jiangsu Province, China
[*]E-mail: yhpang@jiangnan.edu.cn

Thiol biomolecule of glutathione (GSH) combined with lead ion as precursor for synthesis of hierarchical PbS via hydrothermal degradation has been developed. The precursor and as-prepared PbS were characterized by Fourier-transform infrared spectra (FTIR), X-ray diffraction (XRD), scanning electronic microscopy (SEM) and electrochemical technique. Flower-shaped micron crystals, submicron-sized spherical particles and dendritic PbS were controllably synthesized by adjusting pH value of the precursor solutions. GSH acted as both soft template and sulfur source in the synthesis. To investigate the suitability of PbS for pesticidal sensing application, an pesticidal biosensor based on the AChE-CHIT/dendritic PbS/GCE has been devised. Organophosphate pesticide dimethoate was selected as model to examine the feasibility of pesticidal bio-sensing. Under the optimum conditions, a quantitative measurement of dimethoate was achieved with the linear range of 0.05 μM to1.0 μM and the detection limit of 0.02 μM.

1. INTRODUCTION

In recent years submicrometer or nanometer-sized materials have attracted the attention of researchers due to their electronic and optical properties and extensively potential applications [1-4]. Lead sulfide (PbS) is an important π-π semiconductor compound with a rather narrow band gap (0.41 eV at 300 K) and a relatively large excitation Bohr radius (18 nm) [5]. PbS shows extensive quantum-size effects in nanocrystalline form and has wide ranging potential applications, such as solar cells [6-8], electroluminescence [9-10], photoluminescence [11-12], mode-locking in lasers [13], electronic materials [14] and photodetector device [15].

The physical and chemical properties of nanomaterials depend not only on their composition but also on their structure, morphology, phase, shape, size, distribution, and spatial arrangement. Therefore, many nanometer-sized PbS with different morphologies have been synthesized in recent years. For example, cubic-shaped PbS microcrystals and nanocrystals have been produced by the decomposition of a single source precursor [16]. Rodbased PbS multipods were synthesized from the thermal decomposition of a molecular precursor [17]. Star-shaped PbS nanocrystals have been synthesized in aqueous solutions of mixed cationic/anionic surfactants [18]. Unique star-shaped PbS nanocrystals with six symmetric arms along the {100} direction [19], eight symmetric PbS arms along the {111} direction [20], hexapodlike structure of PbS with six symmetric arms [21], regular patterns with truncated octahedrons of PbS nanocrystals [22] were synthesized by chemical methods. Three-dimensional, orthogonal PbS nanowire arrays and networks have been prepared by chemical vapor deposition method [23]. Other structures such as nanoporous nanowire architectures [24], single-crystalline nanowires [25], self-assembled of nanostars patterned arrays [26] were also prepared. And very recently, ultrathin PbS single-crystal sheets were successfully synthesized by chlorine-containing cosolvents directed attachment from nanocrystals [15].

Although above-mentioned structures of PbS have been obtained by various methods, development of water solution-based, conceptually simple, environmentally friendly and large-scale fabrication of hierarchical PbS is still expected in the near future. Biomolecule-assisted synthesis has been proven to be a novel, environmentally friendly, and promising method in the preparation of nanomaterials owing to its convenience and strong function in morphology control. [24, 27-29]. Glutathione (GSH, Scheme 1) is the most important cellular thiol biomolecule, which exists in mammalian cells and creates an important redox system. It is reported that GSH have anticancer activity and it is a main molecule involved in the protection mechanism against itself and against reactive oxygen species generated by metal [30]. GSH has several functional groups, such as –SH, -NH$_2$ and –COOH, which have strong abilities for coordination with the metal ions. The binding of lead (II) by GSH is the subject of interest in toxicity of metal ions in biological system.

In this contribution, we report a GSH-assisted one-step synthesis of hierarchical PbS architectures. The morphology of PbS can be easily modulated by adjusting the pH values of the precursor solutions. Furthermore, a pesticidal biosensor based on the as-synthesized PbS has also been devised. Organophosphate pesticide dimethoate was selected as model target to examine the feasibility of pesticide bio-sensing.
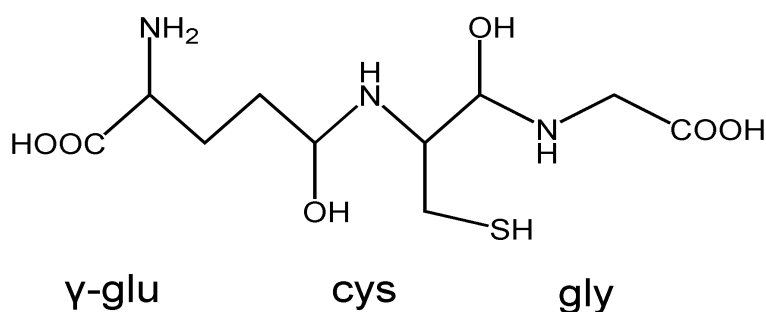
Scheme 1. Structure of L-glutathione (GSH, *g-Glu-Cys-Gly*).

2. EXPERIMENTAL DETAILS

2.1. Reagents

Doubly deionized water (DDW, 18 MΩ cm) was obtained from a WaterPro water purification system (Labconco Corporation, Kansas City, MO, USA).

All chemicals used were of analytical grade and used without further purification. GSH (Sinopharm Chemical reagents, China) and $Pb(CH_3COO)_2 \cdot 3H_2O$ (Tianjin Third Chemicals, China) were used as the starting reactants to prepare the PbS crystals.

Acetylthiocholine chloride (ATCl) and acetylcholinesterase (AChE, type V-S, from Electrophorus electricus, 500 units/mg) were purchased from Aladdin. Dimethoate was the product of J&K Scientific LTD.

2.2. Synthesis of hierarchical PbS architectures

In a typical synthesis, $Pb(CH_3COO)_2 \cdot 3H_2O$ (75.8 mg, 0.2 mmol) and GSH (61.4 mg, 0.2 mmol) were added to 20 mL of doubly deionized water under stirring and then precursor of white precipitant was formed.

The precursor was transferred into a Teflon-lined stainless-steel autoclave. After sealing, the autoclave was maintained at 140 ^{o}C for 24 h and then cooled to room temperature. The black precipitate was collected by centrifugation at 3000 rpm for 3 min and washed three times with pure water and absolute ethanol subsequently to remove ions possibly remaining in the final products. Then the sample was dried under vacuum at room temperature for characterization.

To obtain various morphologies of the final products, the pH values of the precursor have been varied before the synthesis. Acidic and alkaline condition reactions were performed by dropwise addition of acetic acid or 1 M NaOH solution in the precursor respectively until the precursor was dissolved critically.

2.3. Instruments and Characterizations

Fourier-transform infrared (FTIR) spectra (4000-500 cm^{-1}) were recorded with a Magna-560 spectrometer (Nicolet, USA). Powder X-ray diffraction (XRD) pattern was recorded with a D/max-2500 diffractometer (Rigaku Japan) using CuKα radiation (λ=1.5418 Å).

The morphologies and microstructures of the products were characterized on a model SS-550 scanning electron microscope (SEM) at 15.0 kV (Shimadzu, Japan). Electrochemical experiments were carried on a CHI 660C electrochemical workstation (Chenhua Instrument Company, Shanghai, China) with a three-electrode system, a bare glassy carbon electrode (GCE) or a PbS/GCE modified electrode as the working electrode, a saturated calomel electrode (SCE) as the reference electrode and a platinum electrode as the auxiliary electrode.

2.4. Fabrication of AChE-CHIT/dendritic PbS/GCE biosensor

GCE (CH Instrument, diameter = 3 mm) was polished carefully to a mirror-like by use of 0.3 and 0.05 μm alumina slurry and then ultrasonically cleaned in ethanol and ultrapure water. Lastly, the electrode was dried with nitrogen gas.

First, 5.0 μL of PbS was dropped on the pretreated GCE. After drying naturally, 4 μL of mixture of 4 μL AChE and 2 μL chitosan (1 mg/mL) was coated on the PbS modified GCE (PbS/GCE) to form modified electrode (AChE-CHIT/dendritic PbS/GCE). After evaporation of water, the modified electrode was washed with phosphate buffer solution (PBS) to remove the unbound AChE. The prepared AChE-CHIT/dendritic PbS/GCE was stored at 4 ^{o}C when not in use.

2.5. Electrochemical detection of pesticide

The obtained AChE-CHIT/dendritic PbS/GCE biosensor was first immersed in PBS solution (pH 6.5) containing different concentrations of standard dimethoate solution for 10 min, then immediately transferred to electrochemical cell of 5.0 mL pH 6.5 PBS containing 0.2 mM ATCl to study the electrochemical response. The inhibition efficiency ($I\%$) was calculated as follows:

$$I\% = \frac{I_s - I_o}{I_s} \times 100$$

Where I_s and I_o were the steady-state current of ATCl at the AChE-CHIT/dendritic PbS/GCE biosensor before and after pesticide inhibition, respectively.

3. RESULTS AND DISCUSSION

3.1 FTIR of the GSH-Pb

As the GSH is tend to bind with lead(II) in aqueous solution, the complex of GSH with lead ion (GSH-Pb) was employed in this paper for preparation of semiconductor PbS crystals. The formation of GSH-Pb was confirmed by FTIR spectra (as shown in Fig 1). Pure GSH shows a strong band at 2525 cm^{-1} due to V$_{-SH}$, which is absent in the spectra of the GSH-Pb complex. The results indicates the deprotonation and coordination of the thiol group, which suggesting the binding of lead ion through sulphur. The band of GSH at 1714 cm^{-1}, assigned to the >C=O stretching vibration of the -COOH group of the glycine residue, is shifted to lower frequency and merged into a big band. The band shift indicates coordination of -COOH group of glycine with lead ion in the GSH-Pb complex. The band at 1664 cm^{-1} in the GSH, which is assigned to the >C=O stretching of the peptide bonds, has been shifted to lower frequency at 1647 cm^{-1}, indicating the coordination of the >C=O group with lead ion. The N-H stretching frequency at 3027 cm^{-1} in a hydrogen bonded NH^{3+} in zwitter ion of the amino acid moiety does not show any considerable shift in GSH-Pb, indicating the non participation of this N-H group.
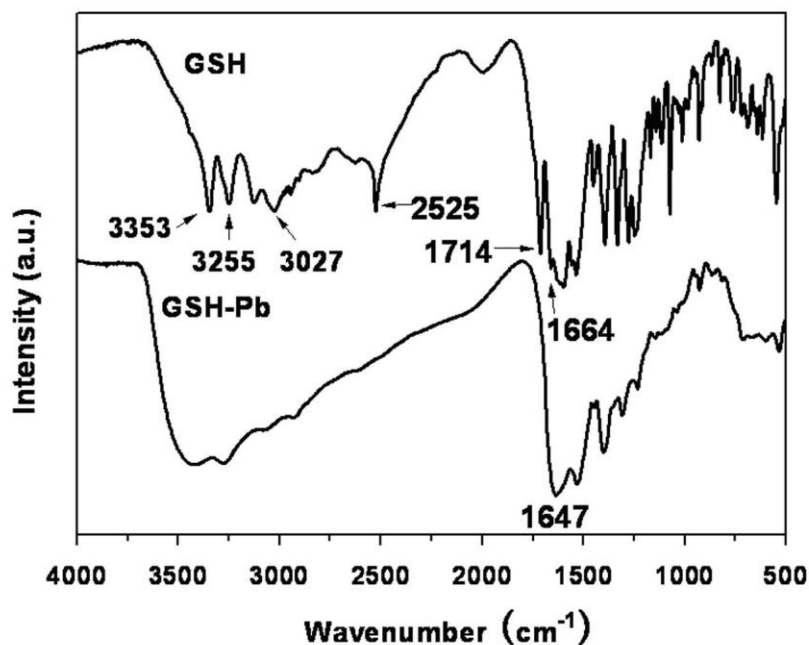
Figure 1. FTIR images of pure GSH (Top) and GSH-Pb complex (Bottom).

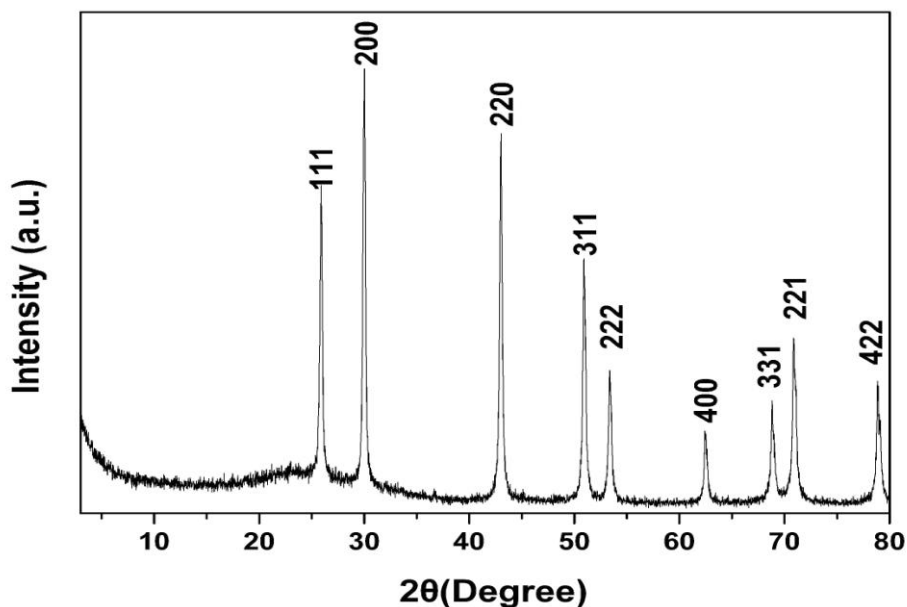*3.2. XRD structural analysis of PbS*

Figure 2. XRD pattern of the as-synthesized PbS crystals.

The transform of GSH-Pb into PbS was carried out under conventional hydrothermal conditions. Powder XRD patterns of the as-obtained black product are shown in Fig. 2. By comparison with the data from JCPDS cards file No. 05-0592, all diffraction peaks can be indexed as a face centered cubic structure of PbS. The strong and narrow peaks show that the material has good crystallite. The XRD patterns confirm that PbS crystallites could be formed with high purity.
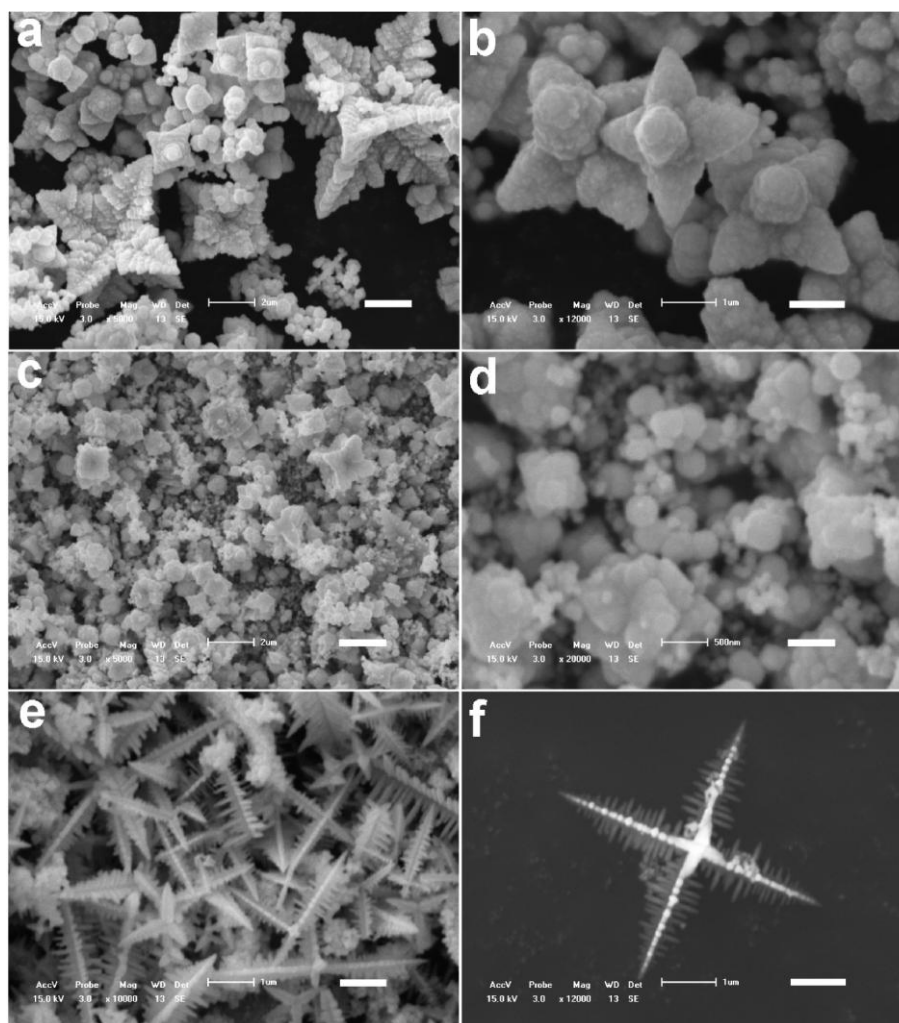
3.3. Morphologies of PbS

Figure 3. SEM images of hierarchical PbS architectures prepared through a hydrothermal reaction at 140 $^\circ$C for 24 h using complex of GSH with lead ions as precursor. The precursor was treated with acetic acid (a, b) pure water (c, d) and NaOH (e, f) respectively. The scale bars in the Fig. 3a-3f are 2 μm, 1 μm, 2 μm, 500 nm, 2 μm and 1 μm, respectively.

The intrinsic properties of nanomaterials are determined not only by their chemical composition but also by their shape and size. So many materials scientists dedicated to design and fabricate artificial crystals with controlled structures [31]. PbS crystals with controllable morphologies were conveniently obtained just by varying pH value of the reaction. Flower-like PbS crystals (Fig. 3a and 3b) were synthesized in an acidic condition by addition of acetic acid in the GSH-Pb precursor solution. The SEM observations show that the flowers have four symmetric petals (Fig. 3a) and some have pistils in the center of flowers as shown in Fig. 3b. It can be seen from SEM images that the length of the symmetrical two petals of the "blossoming flowers" are about 4 μm (showed in Fig. 3a) and the length of those not well blossomed flowers are 1 μm (showed in Fig. 3b). Submicron-sized spherical particles also formed during the hydrothermal treatment. Fig. 3c and 3d gives SEM images of the product that was obtained by hydrothermal treatment only three components: Pb(CH$_3$COO)$_2$, GSH

and H_2O. The morphology of the PbS was significantly changed. The nearly spherically PbS particles and a few flower-like crystals were formed.

When the reaction was performed under alkaline condition by addition of NaOH, the morphology of PbS crystals was greatly changed (showed in Fig. 3e and 3f). The sample has a well-defined dendritic structure and consists of parallel PbS leaflets, which is perpendicular to ridges constituting the dendritic structures. The leaflets extend radically from the ridges. The distance between two neighboring leaflets is about 20 nm. The width of the leaflets is about 50 nm and their length is 100-500 nm varying with changing position on the dendritic structure. The above experimental phenomena further confirmed that the coordination of GSH to lead ions, which is strongly affected by pH conditions, leads to different morphologies of the final PbS crystals.

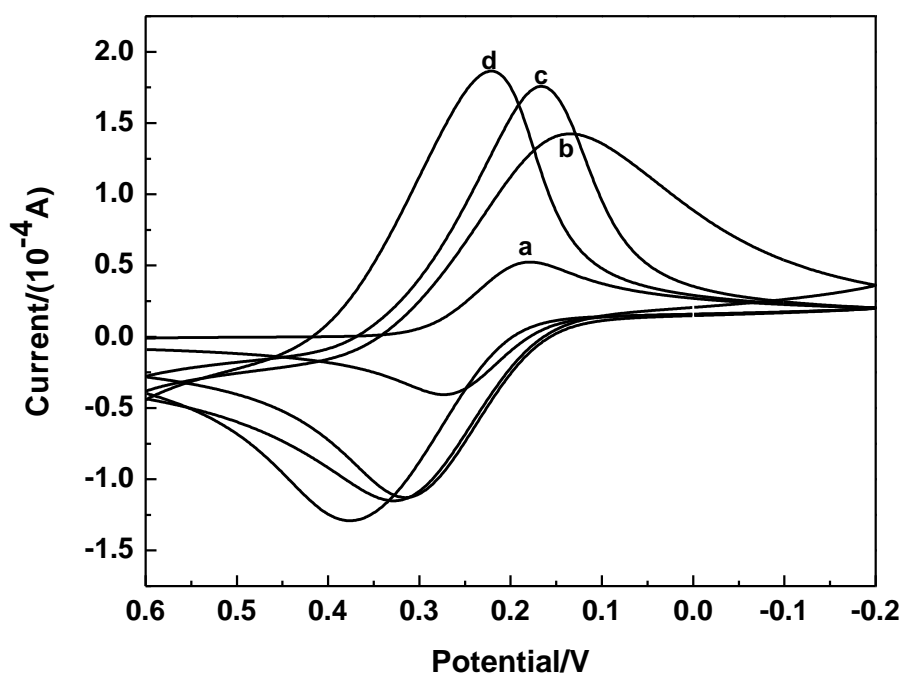*3.4. Electrochemical reactivity of PbS modified electrodes*

Figure 4. cyclic voltammograms of 5 mM $[Fe(CN)_6]^{3-/4-}$ at (a) the bare GCE, (b) flower-like PbS/GCE, (c) spherical PbS/GCE, and (d) dendritic PbS/GCE. Scan rate was 100 mV/s.

Fig. 4 shows the relative CV responses for (a) bare GCE, (b) flower-like PbS modified GCE, (c) spherical PbS modified GCE and (d) dendritic PbS modified GCE in 5mM $Fe(CN)_6^{3-/4-}$ containing 0.1 M KCl solution. It is obvious that, after modified the electrode with different morphologies PbS architectures (Fig. 4. b, c, d), both the oxidation and reduction currents increased dramatically and much higher than that on bare GCE (Fig. 4. a) (the oxidation and reduction peak current on flower-like PbS/GCE enhanced 2.81 and 2.73 times from the respective peak current of the bare GCE. 2.78 and 3.36 times on spherical PbS/GCE. 3.17 and 3.57 times on dendritic PbS/GCE.). The results showed that the introduction of PbS with different morphologies on GCE facilitate the interfacial electron

transfer and amplify electrochemical response in different degrees. The most remarkably enhancement of electrochemical signals was obtained at dendritic PbS/GCE. Therefore, dendritic PbS was selected to fabricate pesticidal biosensor.

3.5. Optimization of experimental parameters
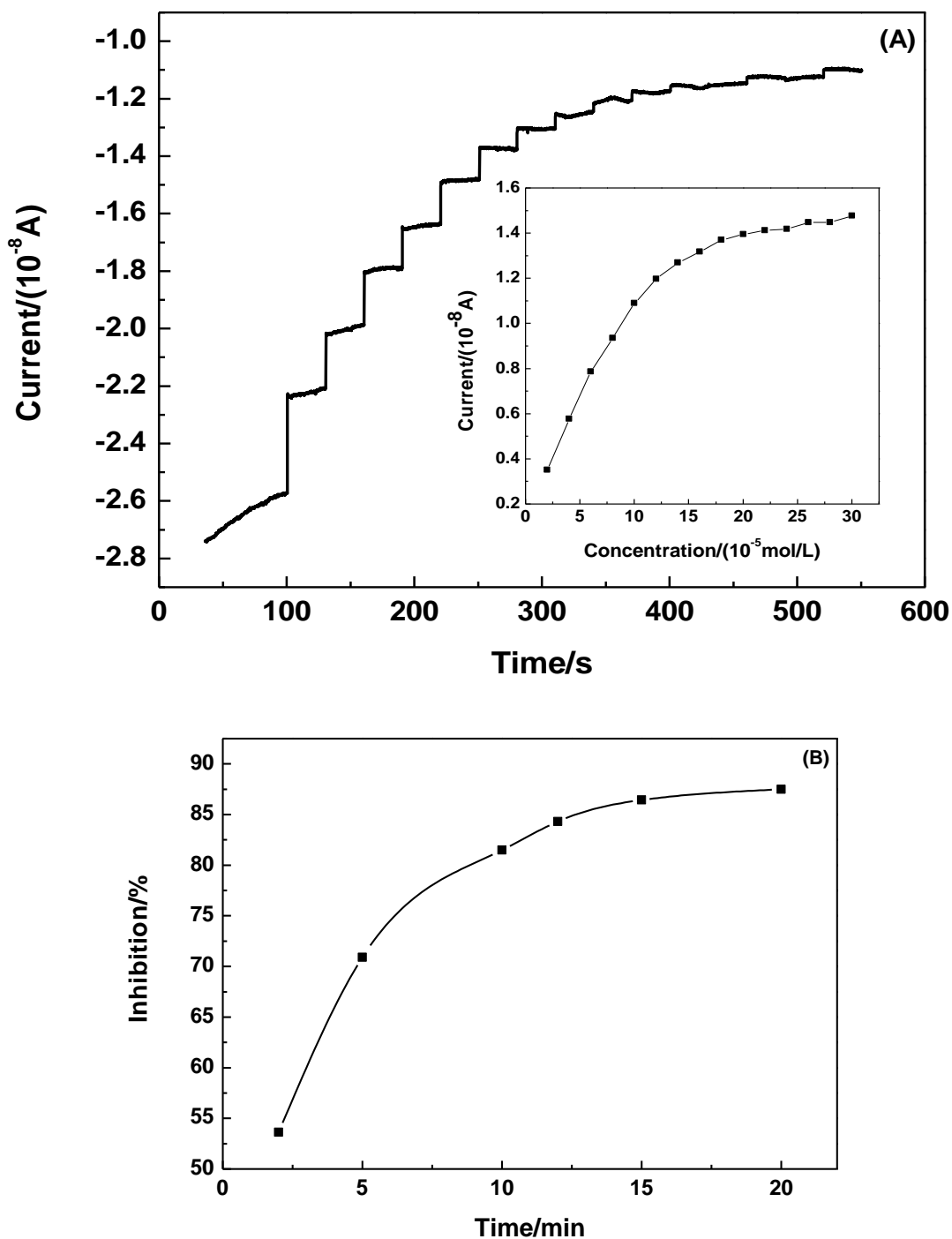

Figure 5. Effects of (A) ATCl concentration and (B) inhibition time on the response of AChE/ dendritic PbS/GCE biosensor.

The effect of ATCl concentration on the response of the AChE-CHIT/dendritic PbS/GCE was observed. Fig. 5A showed a typical current–time plot of AChE-CHIT/ dendritic PbS/GCE biosensor after successive addition of ATCl under stirring every 30 s.
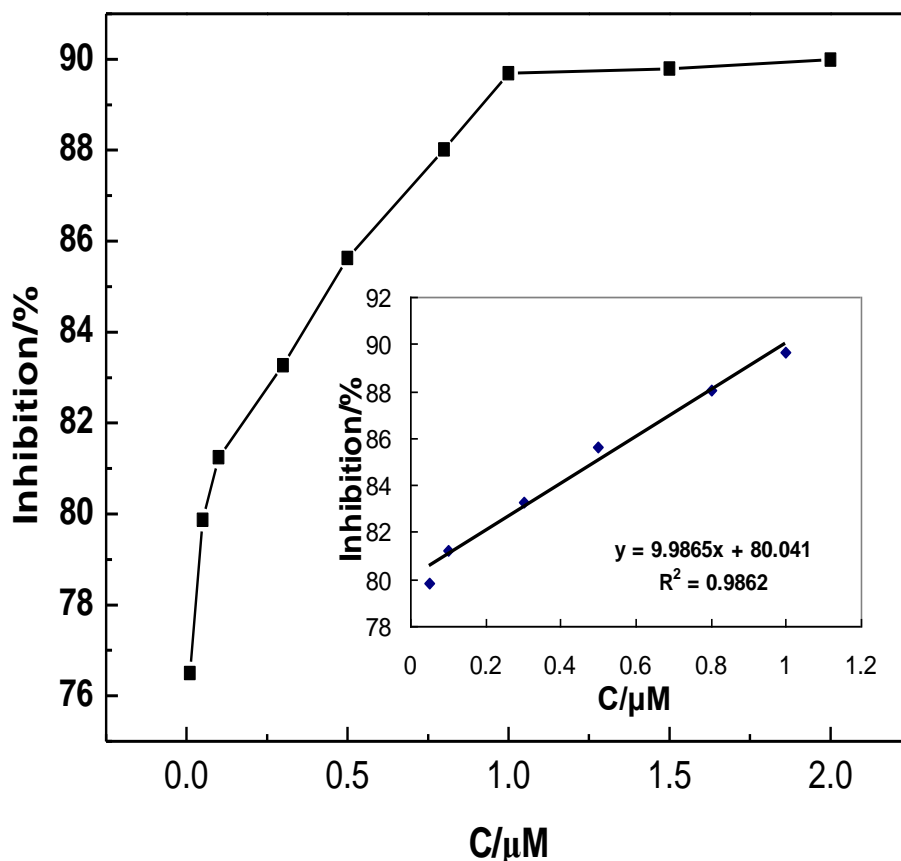

Figure 6. Inhibition curve of the AChE-CHIT/dendritic PbS/GCE biosensor to different dimethoate concentrations (0.01, 0.05, 0.1, 0.3, 0.5, 0.8, 1.0 1.5, 2.0 μM). Insets show the calibration curve for dimethoate determination.

With each addition of ATCl, the biosensor could achieve the steady-state current within 0.58 s, which indicated a fast electron transfer process. When the concentration of ATCl was higher than 200 μM, a plateau was observed. So ATCl concentration was chosen as 200 μM in this paper. This curve showed a characteristic of the Michaelis–Menten relationship. The apparent Michaelis–Menten constant (K_M^{app}) is a reflection of both the enzymatic affinity and the ratio of microscopic kinetic constants. According to the Lineweaver–Burk equation, the K_M^{app} value was calculated to be 0.11 mM. This value was lower than that of 0.18 mM for AChE–AuNPs–SF/Pt [32], 0.22 mM for AChE–CHO/PAMAM/Au [33], 0.45 mM for AChE/AuNPs–CS–SiSG/GCE [34], indicating that the immobilized AChE on PbS/GCE presented here had a greater affinity to ATCl.

Inhibition time is one of the most influential parameters in pesticide analysis. With an increase of immersion time in the dimethoate solution, the peak current of ATCl on the AChE-CHIT/dendritic

PbS/GCE was decreased greatly. As shown in Fig. 5B, dimethoate displayed an increasing inhibition on AChE with the immersion time increased. When the immersion time was longer than 10 min, the curve tended to a stable value, indicating the binding interactions with active target groups in the enzyme reached saturation. This change tendency of the peak current reflects an alteration of enzymatic activity, in turn resulting in the change of the interactions with its substrate. Thus 10 min incubation time is chosen for the subsequent experiments for the dimethoate concentration determination.

3.6 Determination of Dimethoate Concentrations

With increasing the concentration of dimethoate in the immersion solution, the produced current of ATCl on the AChE-CHIT/dendritic PbS/GCE decreased greatly. As shown in Fig. 6, its inhibition curve tended towards maximum values at high pesticides concentrations, indicating that interactions with active target groups reached saturation as the pesticides concentration increased. Under the optimized experimental conditions, the dimethoate inhibition to AChE-CHIT/dendritic PbS/GCE was proportional to its concentration in the range from 0.05 μM to1.0 μM. The detection limit was calculated to be 0.02 μM.

In addition, the stability of the enzyme electrode could be maintained by being stored at 4 °C in dry condition. No obvious decrease in the response of ATCl was observed in the first 3-weeks storage. After a 6-weeks storage period, the sensor still retained 87% of its initial current response.

4. CONCLUSIONS

In this paper, a facile process based on a conventional hydrothermal treatment of chelate of GSH with lead ions has been developed to selectively and controllably synthesize PbS crystals with flower-like structures, submicron-sized spherically particles and dendritic structures. No soft template and additional sulfur source was needed during the synthesis. The mobilization of PbS on GCE facilitate the interfacial electron transfer. Different morphologies of PbS modified on GCE would amplify electrochemical response in different degrees. A pesticidal biosensor based on AChE-CHIT/dendritic PbS/GCE was devised for determination of organophosphate pesticide dimethoate. To sum up, this study provides a promising route for the facile and cost-effective synthesis of nano- and micro- PbS, and the as-synthesized materials showed great potential in pesticidal electrochemical bio-sensing.

References

1. S. Mann, *Nat. Mater.,* 8 (2009) 781.
2. J. S. Jie, W. J. Zhang, I. Bello, C. S. Lee, S. T. Lee, *Nano Today,* 5 (2010) 313.
3. J. H. Bang, K. S. Suslick, *Adv. Mater.*, 22 (2010) 1039.
4. A.Bonanni, T. Dietl, *Chem. Soc. Rev.,* 39 (2010) 528.
5. F. W. Wise, *Acc. Chem. Res.,* 33 (2000) 773.
6. R. Plass, S. Pelet, J. Krueger, M. Gratzel, U. Bach, *J. Phys. Chem. B,* 106 (2002) 7578.
7. N. Zhao, T. P. Osedach, L. Y. Chang, S. M. Geyer, D. Wanger, M. T. Binda, A. C. Arango, M. G. Bawendi, V. Bulovic, *Acs Nano,* 4 (2010) 3743.
8. T. Ju, R. L. Graham, G. M. Zhai, Y. W. Rodriguez, A. J. Breeze, L. L. Yang, G. B. Alers, S. A. Carter, *Appl. Phys. Lett.*, 97 (2010) 043106.
9. L. Bakueva, S. Musikhin, M. A. Hines, T.W. F. Chang, M. Tzolov, G. D. Scholes, E. H. Sargent, *Appl. Phys. Lett.,* 82 (2003) 2895.
10. L. F. Sun, L. Bao, B. R. Hyun, A. C. Bartnik, Y. W. Zhong, J. C. Reed, D. W. Pang, H. D. Abruna, G. G. Malliaras, F. W. Wise, *Nano Lett.,* 9 (2009)789.
11. N. O. Dantas, F. Qu, R. S. Silva, P. C. Morais, *J. Phys. Chem. B,* 106 (2002) 7453.
12. T. Zhang, H. G. Zhao, D. Riabinina, M. Chaker, D. L. Ma, *J. Phys. Chem. C,* 114 (2010) 10153.
13. G. Tamulaitis, V. Gulbinas, G. Kod*is, A. Dementjev, L. Valkunas, I. Motchalov, H. Raaben, J. Appl. Phys.,* 88 (2000) 178.
14. W. Li, J. F. Chen, T. Wang, *Physica B,* 405 (2010) 1279.
15. C. Schliehe, B. H. Juarez, M. Pelletier, S. Jander, D. Greshnykh, M. Nagel, A. Meyer, S. Foerster, A. Kornowski, C. Klinke, H. Weller, *Science,* 329 (2010) 550.
16. T. Trindade, P. O'Brien, X. M. Zhang, M. Motevalli, *J. Mater. Chem.,* 7 (1997) 1011.
17. S. M. Lee, W. W. Jun, S. N. Cho, J. Cheon, *J. Am. Chem. Soc.,* 124 (2002) 11244.
18. N. N. Zhao, L. M. Qi, *Adv. Mater.,* 18 (2006) 359.
19. S .M. Lee, Y. W. Jun, S. N. Cho, J. Cheon, *J. Am. Chem. Soc.,* 124 (2002) 11244.
20. Y. Ma, L. Qi, J. Ma, H. Cheng, *Cryst. Growth Des.,* 4 (2004) 351.
21. Y. H. Zhang, L. Guo, P. G. Yin, R. Zhang, Q. Zhang, S. H. Yang, *Chem. Eur. J.,* 13 (2007) 2903.
22. N. Wang, X. Cao, L. Guo, S. H. Yang, Z. Y. Wu, *ACS Nano.,* 2 (2008) 184.
23. J. P. Ge, J. Wang, H. X. Zhang, X. Wang, Q. Peng, Y. D. Li, *Chem. Eur. J.,* 11 (2005) 1889.
24. X. F. Shen, X. P. Yan, *J. Mater. Chem.,* 18 (2008) 4631.
25. S. Y. Jang, Y. M. Song, H. S. Kim, Y. J. Cho, Y. S. Seo, G. B. Jung, C. W. Lee, J. Park, M. Jung, J. Kim, B. Kim, J. G. Kim, Y. J. Kim, *Acs Nano,* 4 (2010) 2391.
26. T. Huang, Q. A. Zhao, J. Y. Xiao, L. M. Qi, *Acs Nano,* 4 (2010)4707.
27. S. L. Xiong, B. J. Xi, D. C. Xu, C. M. Wang, X. M. Feng, H. Y. Zhou, Y. T. Qian, *J. Phys. Chem. C,* 111(2007) 16761.
28. F. Zuo, S. Yan, B. Zhang, Y. Zhao, Y. Xie, *J. Phys. Chem. C,* 112(2008) 2831.
29. H. Tong, Y. J. Zhu, L. X. Yang, L. Li, L. Zhang, *Angew. Chem. Int. Ed.,* 45(2006) 7739.
30. B. K. Singh, R. K. Sharma, B. S. Garg, *J. Therm. Anal. Calorim.,* 84 (2006) 593.
31. Y. N. Xia, Y. J. Xiong, B. Lim, S. E. Skrabalak, *Angew. Chem. Int. Ed.,* 48(2009) 60.
32. H.S. Yin, S.Y. Ai, J. Xu, W.J. Shi, L.S. Zhu, *J. Electroanal. Chem.,* 637 (2009) 21.
33. M. Snejdarkova, L. Svobodova, G. Evtugyn, H. Budnikov, A. Karyakin, D.P. Nikolelis, T. Hianik, *Anal. Chim. Acta,* 514 (2004) 79.
34. D. Du, S. Chen, J. Cai, D. Song, *J. Electroanal. Chem.,* 611 (2007) 60.